PERGAMON

International Journal of Heat and Mass Transfer 42 (1999) 4461–4474

International Journal of HEAT and MASS TRANSFER

www.elsevier.com/locate/ijhmt

Effects of leading-wall blowing/suction on mixed convective phenomena in a radially rotating multiple-pass duct

Jenn-Jiang Hwang[a,*], Yeong-Pei Tsai[a], Wei-Jyh Wang[a], Dong-Yu Lai[b]

[a] *Department of Mechanical Engineering, Chung-Hua University, Hsinchu, Taiwan 300, ROC*
[b] *Air Force Aeronautics Technology School, Kangshan, Kaohsiung, Taiwan 820, ROC*

Received 17 August 1998; received in revised form 23 March 1999

Abstract

A numerical study is performed to examine the transpiration-wall effect on mixed convection in a radially rotating multi-pass square duct connected with 180° sharp returns. Uniform injection or suction is applied to the leading wall of the rotating duct. Finite-difference method is adopted to solve three-dimensional Navier–Stokes equations and the energy equation. Periodic conditions are used between the entrance and exit of a typical two-pass duct for the closure of the elliptic problem. As predicted, results show that the radial distance from the rotational axis to initiation of flow reversal in the radial-outward duct (ROD) decreases with increasing rotational buoyancy. The appearance of flow reversal is delayed by the leading-wall blowing but is quickened by the leading-wall suction. The wall-blowing rate for avoiding the flow reversal in the ROD increases with increasing rotational buoyancy. Moreover, the axial distribution of peripherally averaged Nusselt number is closely related to the development of cross-flow intensity. They are increased/decreased with increasing the wall blowing/suction rate in the ROD but are essentially unaltered in the radial-inward duct (RID).

1. Introduction

This paper studies the effect of leading-wall transpiration on the mixed convection in a rotating multiple-pass duct, which is closely but not restrictedly related to the transpiration cooling of turbine blades. It is also valuable for many practical applications or problems such as mass transfer, drying, ablation, and boundary-layer control in a rotating system.

In the past three decades, fluid flow and heat transfer in radially rotating single-pass ducts had been studied extensively. Only some relevant works are cited below. Hart [1], Ito and Nanbu [2], Moore [3,4], Spezial and Thangam [5], and Kheshgi and Scriven [6] examined the effect of Coriolis force on the adiabatic fluid flow in radially rotating single-pass ducts. The Coriolis-induced secondary flow had been well documented in these investigations. References [7–15] are a series of studies in which the effect of rotation on the developing and/or fully developed heat transfer in radially rotating single-pass ducts is examined. The general conclusion drawn from these investigations was that the trailing-side heat transfer was higher than the corresponding stationary value; while the leading-side heat transfer was severely suppressed by rotation.

Recently, Wagner et al. [16,17], Yang et al. [18], and Hwang and Kuo [19] carried out the experimental measurements on the convective heat transfer in radially rotating serpentine-shaped multiple-pass passages. Hwang and Lai [20,21] performed numerical studies of the fluid flow and heat transfer in a radially

* Corresponding author. Tel.: +886-35-374281, ext. 8334; fax: +886-35-373771.
E-mail address: jjhwang@chu.edu.tw (J.J. Hwang)

0017-9310/99/$ - see front matter
PII: S0017-9310(99)00110-6

Nomenclature

A_L	total leading surface area
A_p	cross-sectional area at duct entrance
AR	area ratio of the total heat transfer surface of the module and the duct cross section
De	duct hydraulic diameter [m]
G	mass flow rate [kg s^{-1}]
Gr	rotational Grashof number, $\Omega^2 L_x \beta_T q_w De^4/(\nu^2 k_f)$
k_f	air thermal conductivity [kW m^{-1} K^{-1}]
L_x	characteristic length in radial direction (in term of duct hydraulic diameter, De) [m]
Nu_s	Nusselt number for fully developed laminar flow in square duct
Nu_x	local Nusselt number, Eq. (13)
P, p	dimensionless and dimensional pressure
Pi	module pitch in z-direction, i.e., $3De$ [m]
Pr	Prandtl number
q_w	wall heat flux [kW m^{-2}]
Q	total heat input into the module [kW]
Re	Reynolds number, $\overline{w}De/\nu$
Ri	Richardson number, Gr/Re^2
Ro	rotation number, $\Omega De/\overline{w}$
T	temperature [K]
T_b	local bulk mean temperature of air [K]
T_w	local wall temperature [K]
u, v, w	local velocities in X-, Y- and Z-directions, respectively [m s^{-1}]
U, V, W	dimensionless local velocities in X-, Y- and Z-directions, respectively
$\overline{w}$	average flow velocity at the duct inlet [m s^{-1}]
x, y, z	rectangular coordinate [m]
X, Y, Z	dimensionless rectangular coordinate, see Fig. 1
X_0, x_0	dimensionless and dimensional radial distance from the rotation axis to the module.

Greek symbols

β	dimensionless pressure drop parameter [kPa m^{-1}]
β_T	thermal expansion coefficient [K^{-1}]
γ	dimensionless air enthalpy rise parameter, $Q/(Gc_pPi)$
η	dimensionless mass increase parameter, $v_w A_L/(3A_p\overline{w})$
ϑ	dimensionless temperature, $(T-T_r)/(q_w De/k_f)$
ν	kinematic viscosity [m^2 s^{-1}]
ρ	air density [kg m^{-3}]
σ	cross-sectional averaged cross-flow intensity, Eq. (14)
Ω	angular rotation speed [s^{-1}].

Subscripts

b	bulk mean
f	fluid
L	leading wall
r	reference
s	smooth, stationary or static
w	wall.

Superscripts

$\hat{}$	periodicity
$\bar{}$	average
$*$	with dimension.

rotating multiple-pass duct. In general, heat transfer mechanisms in a radially rotating multiple-pass duct are very complicated due to the Coriolis force, the rotation-induced buoyancy, and their interaction. Coriolis force augments and degrades the heat transfer on high-pressure and low-pressure surfaces, respectively [16–20]; while the heat transfer benefits of the buoyancy depend on the directions of radial flow [16,20].

As for the wall-transpiration effect, which was not considered in any of the above studies, Soong and Hwang [22] solved the fluid flow and heat transfer in a radially rotating two-dimensional plate channel with semiporous walls by using the similarity method. The height-to-width aspect ratio was assumed to be small in order to neglect the side effect. Yan [23] studied numerically the effect of trailing-wall suction on the forced convection in a radially rotating duct with outward flow. The effect of rotation-induced buoyancy was not considered in the work. Yan [24] then extended his work [23] to examine the buoyancy effect on the mixed convection in a radially rotating duct with wall transpiration. However, only radially outward flow was considered.

As indicated by the above review of previous efforts, the study of fluid flow and heat transfer in radially rotating multiple-pass ducts of solid walls is rather sparse, let alone the transpiration walls. It is thus the purpose of this study to examine the effect of leading-wall transpiration on mixed convection in a rotating

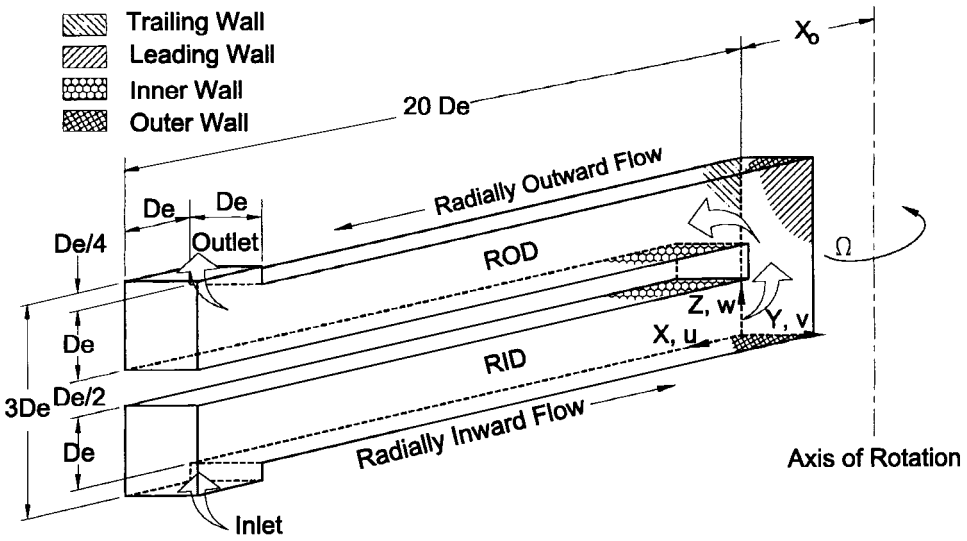

Fig. 1. Configuration, dimensions and coordinates of the test module.

multiple-pass channel. Two objectives are to be obtained by this study. First, we study the buoyancy effect on the flow-reversal phenomena in a serpentine duct of solid walls by varying the wall heat flux. It is well known that the radial outward flows will reverse themselves under high against buoyancy conditions [20,25]. The fluid is nearly stagnant when the radial flow begins to reverse, which, in turn, causes the heat transfer to degrade considerably. From the viewpoint of thermal design of internal cooling of the rotating passages, it is very important to understand the relation between the rotational buoyancy and the flow-reversal phenomena. Second, to deal with the flow reversal, we examine the leading-wall blowing/suction effect on the flow reversal in the radial duct, subsequently control the flow reversals, and prevent the local hot spots.

2. Analysis

2.1. Physics of the problem

A schematic of the present problem is shown in Fig. 1. Since the serpentine-duct geometry contains identical two-pass modules, the flow is expected to attain, after an entrance duct, a periodic fully developed regime, in which the thermal-fluid properties, via a proper analysis, repeat themselves from module to module. It is thus possible to calculate the flow and heat transfer in a typical two-pass module, without the need for the entrance region calculation. This obviously not only reduces considerably the computational effort but also ignores the relatively difficult task of solving the entrance-region problem. As shown in Fig. 1, the periodic two-pass module contains a radially inward duct, a radially outward duct, and two 180° sharp turns. It rotates at a constant angular speed Ω about the axis in parallel with z-direction. The duct of square cross-section is $20De$ in radial length, and the distance from the axis of rotation to the test module is fixed at $x_0 = 10De$. For simplicity, the radially inward duct and

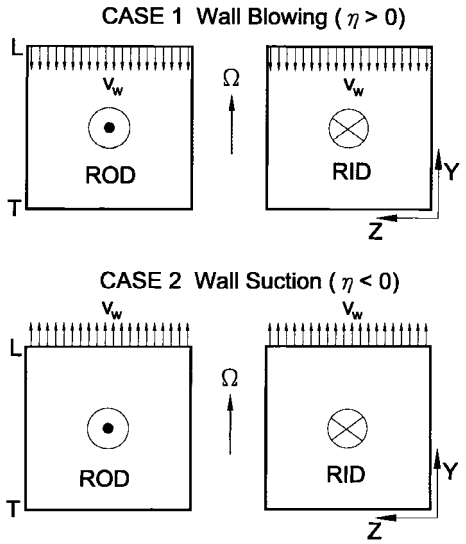

Fig. 2. Investigated boundary conditions on the leading wall: (a) blowing; (b) suction.

the radially outward duct are abbreviated as 'RID' and 'ROD', respectively, in the following discussion. In addition, on the leading wall of the entire module, as shown in Fig. 2, some fluid with a uniform velocity v_w is either injected into the duct or sucked away from the duct.

The rotation induced centrifugal inertia on the fluid particles in a given radial plane is represented by $-\rho\Omega^2(x+x_0)$. In the absence of density variation in an incompressible flow, the centrifugal force is hydrostatic and it only modifies the pressure. However, in the case of heated walls, a temperature gradient exists from the wall region to the core, which gives rise to the centrifugal buoyancy. By quoting the Boussinesq approximation of a linear density-temperature relation, i.e., $\rho=\rho_0[1-\beta_T(T-T_0)]$, the centrifugal buoyancy acting on a radial plane becomes $-\rho\beta_T(T-T_0)(x_0+x)\Omega^2$. In addition, the Coriolis forces driving the flow in the x- and y-directions are $2v\Omega$, and $-2u\Omega$, respectively. To facilitate the analysis, the flow is assumed to be steady and with constant properties, and the axial diffusion, viscous dissipation, and compression work are all ignored. Moreover, gravitational inertia is neglected due to its small magnitude compared to the rotational induced centrifugal force.

2.2. Governing equations

In the subsequent discussion, a general formulation according to the concepts of periodic fully developed flow and heat transfer is developed to accommodate the periodic two-pass duct. Basically, the test section shown in Fig. 1 can be regarded as a 'periodically varied cross-section area' module in z-direction; therefore, the physical quantities are decomposed in z-direction. According to Patankar et al. [26], the pressure p and temperature T of a periodically fully developed flow can be decomposed as

$$p(x,y,z)=-\beta^* z+\hat{p}(x,y,z) \tag{1}$$

$$T(x,y,z)=\gamma^* z+\hat{T}(x,y,z) \tag{2}$$

where both the global pressure drop parameter $\beta^*=[p(x,y,z)-p(x,y,z+Pi)]/Pi$ and the temperature increase parameter $\gamma^*=[T(x,y,z+Pi)-T(x,y,z)]/Pi$ are constants. The quantities of $\hat{p}$ and $\hat{T}$ identically repeat themselves from module to module. That is,

$$\hat{p}(x,y,z)=\hat{p}(x,y,z+Pi)=\hat{p}(x,y,z+2Pi)=\cdots \tag{3}$$

$$\hat{T}(x,y,z)=\hat{T}(x,y,z+Pi)=\hat{T}(x,y,z+2Pi)=\cdots \tag{4}$$

Since uniform flow is either injected into or sucked away from the radial duct, the total mass flow rate across the duct should be either increased or decreased along the module width direction. The discrepancy of the velocity magnitude w between the exit and entrance of each two-pass module should be identical, i.e.,

$$w(x,y,z+Pi)-w(x,y,z)=w(x,y,z+2Pi)-w(x,y,z+Pi)=\cdots \tag{5}$$

Accordingly, a periodical velocity $\hat{w}$ and the velocity increment can be represented as

$$w(x,y,z)=\eta^* z+\hat{w}(x,y,z) \tag{6}$$

where η^* is a mass increase parameter and is defined as

$$\eta^*=\frac{w(x,y,z+Pi)-w(x,y,z)}{Pi}=\frac{v_w A_L}{Pi A_p} \tag{7}$$

A_L and A_p are the total leading-surface area of a two-pass module and the cross sectional area at the duct entrance, respectively. Referring to the coordinate system shown in Fig. 1 and dimensionless parameters of $X=x/De$, $Y=y/De$, $Z=z/De$, $U=u/\overline{w}$, $V=v/\overline{w}$, $W=w/\overline{w}$, $\vartheta=k_f(\hat{T}-T_r)/(q_w De)$, $\hat{P}=\hat{p}/(\rho\overline{w}^2)$, $\beta=\beta^* De/(\rho\overline{w}^2)$, $\gamma=AR/(3Re\ Pr)$, $\eta=\eta^* De/\overline{w}=v_w A_L/(3A_p\overline{w})$, $Re=\overline{w}De/\nu$, $Ro=\Omega De/\overline{w}$ and $Ri=\Omega^2\beta_T q_w De^3/(k_f\overline{w}^2)$, the equations governing the mass, momentum and energy can be written as

$$\frac{\partial U}{\partial X}+\frac{\partial V}{\partial Y}+\frac{\partial \hat{W}}{\partial Z}+\eta=0 \tag{8}$$

$$U\frac{\partial U}{\partial X}+V\frac{\partial U}{\partial Y}+(\hat{W}+\eta Z)\frac{\partial U}{\partial Z}=-\frac{\partial \hat{P}}{\partial X}+\frac{1}{Re}\left(\frac{\partial^2 U}{\partial X^2}+\frac{\partial^2 U}{\partial Y^2}+\frac{\partial^2 U}{\partial Z^2}\right)+2RoV-Ri\,\vartheta(X+X_0) \tag{9}$$

$$U\frac{\partial V}{\partial X}+V\frac{\partial V}{\partial Y}+(\hat{W}+\eta Z)\frac{\partial V}{\partial Z}=-\frac{\partial \hat{P}}{\partial Y}+\frac{1}{Re}\left(\frac{\partial^2 V}{\partial X^2}+\frac{\partial^2 V}{\partial Y^2}+\frac{\partial^2 V}{\partial Z^2}\right)-2RoU-Ri\,\vartheta Y \tag{10}$$

$$U\frac{\partial \hat{W}}{\partial X}+V\frac{\partial \hat{W}}{\partial Y}+(\hat{W}+\eta Z)\frac{\partial(\hat{W}+\eta Z)}{\partial Z}=-\frac{\partial \hat{P}}{\partial Z}+\beta+\frac{1}{Re}\left(\frac{\partial^2 \hat{W}}{\partial X^2}+\frac{\partial^2 \hat{W}}{\partial Y^2}+\frac{\partial^2 \hat{W}}{\partial Z^2}\right) \tag{11}$$

$$U\frac{\partial \vartheta}{\partial X}+V\frac{\partial \vartheta}{\partial Y}+(\hat{W}+\eta Z)\frac{\partial \vartheta}{\partial Z}=\frac{1}{Re\,Pr}\left(\frac{\partial^2\vartheta}{\partial X^2}+\frac{\partial^2\vartheta}{\partial Y^2}+\frac{\partial^2\vartheta}{\partial Z^2}\right)-\gamma(\hat{W}+\eta Z) \quad (12)$$

2.3. Boundary conditions

Except for the leading wall, all duct walls have no slips, i.e., $U=V=W=0$. Uniform suction or blowing is applied to the leading wall, i.e., $V=\pm v_w/\overline{w}$ and $U=W=0$ at $Y=0$. In addition, each duct wall of the module is heated uniformly, i.e., $\partial\vartheta/\partial n=1$, where n denotes the dimensionless coordinate normal to the duct wall. At the module inlet and outlet, the periodicity is applied for the pressure, velocity and temperature components, i.e., $\Phi(X, Y, Z)=\Phi(X, Y, Z+3)$, where Φ may be $\hat{P}$, U, V, $\hat{W}$ and ϑ.

2.4. Solution procedure

The governing equations are numerically solved by the control-volume-based finite difference method [27]. The discretization procedure ensures conservation of mass, momentum, and energy over each control volume. Velocity control volumes are staggered with respect to the main control volumes, and coupling of the pressure and velocity fields is treated via the SIMPLER [27,28] pressure correction algorithm. The smooth hybrid central/skew upstream difference scheme [29] is used to treat the diffusion and convective terms. Obtaining new values for any desired variables, taking into account the latest known estimated values of the variable from the neighboring nodes solves the set of the differential equations over the entire region. One iteration process is complete when, in line-by-line technique, all lines in a direction have been accounted for. Because of the large variations in the source terms, under-relaxation is necessary for the dependent variables and the source terms to achieve convergence. Line inversion iteration with typical under-relaxation values of 0.5 for the velocity terms and 0.7 for the pressure correction term are incorporated to the facilitated calculation. Solutions are considered to be converged at each test condition after the ratio of residual source (including mass, momentum, and energy) to the maximum flux across a control surface becomes below 1.0×10^{-3}.

The computations are processed in the following order:

1. Specify the duct throughflow rate (Re), rotating speed (Ro), wall heat flux (γ, Ri) and wall blowing/suction rate (η) in the serpentine duct, and then guess a corresponding pressure-drop parameter β.
2. Assign the values of U, V, $\hat{W}$ and ϑ, and the parameters at the module inlet and outlet.
3. Solve the momentum and energy equations with the guessed pressure fields.
4. Correct the pressures and velocities everywhere through SIMPLER algorithm until converged.
5. Solve the energy equation for the temperature.
6. Check the mass conservation between the module entrance and exit. If the mass is not conserved, by using trial-and-error, guess a new value of the pressure-drop parameter β.
7. Repeat steps 2–6 until the mass is conserved.

2.5. Grid test

All computations are performed on $72\times20\times50$ (X by Y by Z) straight-line grids in the present work. Additional runs for the coarser meshes, $50\times12\times30$, and the finer meshes, $90\times30\times70$, are taken for a check of grid independence. The parameters used to check the grid independence are axial velocity profile, temperature profile, and the local Nusselt number distribution. Fig. 3 shows the comparison of axial velocity profiles at $X=10$ for $Re=1000$, $Ri=0.04$, and $\eta=0$ among the three grid sizes. The differences of U between two succeeding grids shown in this figure become small, confirming that the results are converging toward the grid independent solution. Computations for $\eta=0.0548$ are also conducted and the results indicate a maximum change of 1.2% in Nusselt number distribution between the solutions of $72\times20\times50$, and $90\times30\times70$ grids. These changes are so small that the accuracy of the solutions on the set of grid $72\times20\times50$ is deemed satisfactory.

Numerical computations of the periodical flows are difficult due to the fact that no boundary information is available in the main flow direction along which the discretization coefficients are large. Partly due to this reason, the code takes as high as 5000 to 9000 iterations for convergence. On Convex-C3840, this is translated to about 8 to 20 h of CPU time.

3. Results and discussions

3.1. Buoyancy-driven flow reversal

Fig. 4 shows a typical development of axial velocity in a periodical rotating two-pass duct of solid walls, which serves as a comparison base to examine the effects of wall suction and blowing. The flow conditions are fixed at $Re=1000$, $Ro=0.1$ and $Ri=0.03$. The plot is viewed in the direction to the rotating axis (i.e., negative x). The solid and dashed curves represent the forward and reversed flows, respectively. The number on the graph represents the

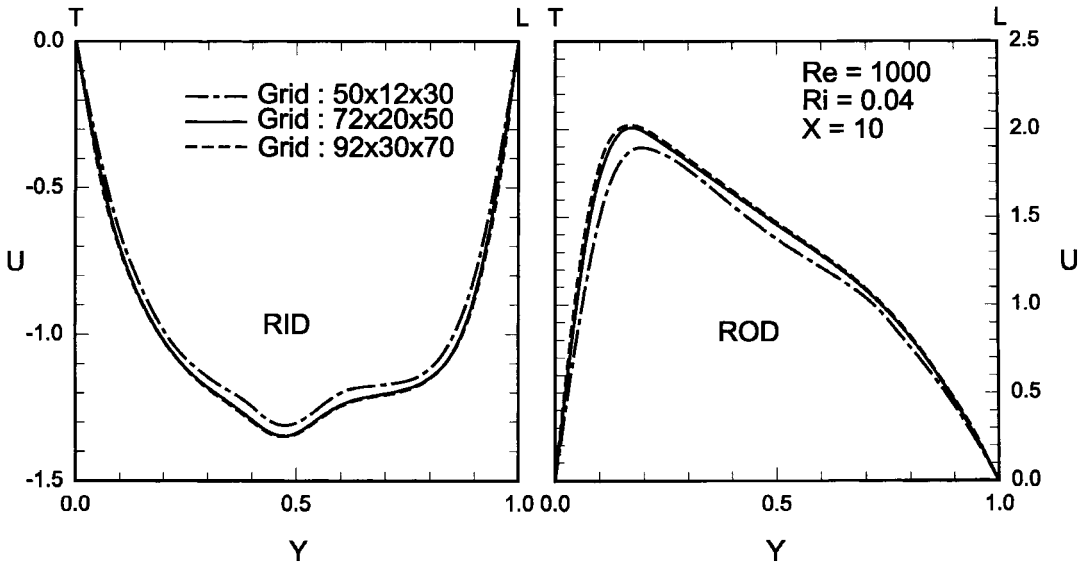

Fig. 3. Grid test by comparing the radial velocity at $X = 10$.

value of non-dimensional velocity (U). Basically, the rotation-induced Coriolis force as well as the buoyancy force affects the flow structures in the RID and ROD. The detailed description of their effects had been provided elsewhere [20] and only some important features are stressed here. Physically, as shown in Fig. 4, the Coriolis force places the high-velocity cores to the leading and trailing walls of the RID and ROD, respectively. In addition, the rotation-induced buoyancy directing radial fluid to the rotational axis aids and impedes the radial flows in the RID and ROD, respectively. Obviously, due to against buoyancy in the ROD, the flow reversal occurs adjacent to the leading wall after $X = 10$. To prevent the large deterioration of heat transfer performance resulting from the flow reversal [20], an examination of the wall blowing/suc-

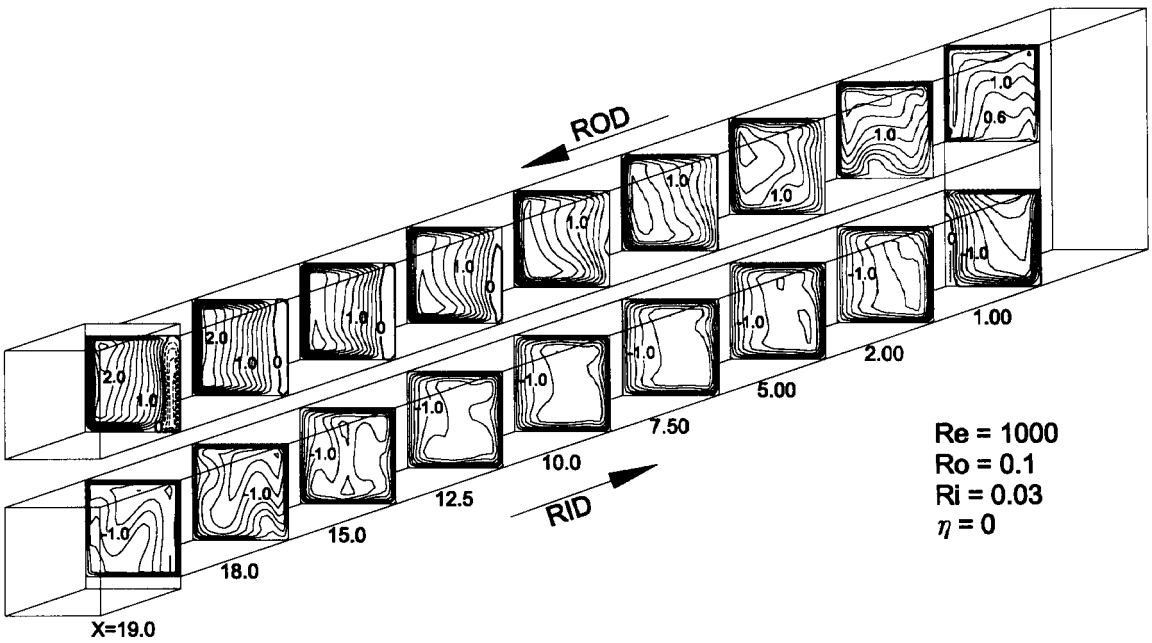

Fig. 4. Development of axial flow along the radial distance of the solid-walled duct ($\eta = 0$) for $Ri = 0.03$, $Ro = 0.1$ and $Re = 1000$.

tion effect on the fluid flow and heat transfer in a rotating serpentine duct is undertaken as follows.

3.2. Effects of wall blowing and suction

The effects of wall blowing and suction on the development of radial velocity along axial distance of the two-pass duct are shown in Figs. 5 and 6, respectively. The rotating and buoyancy conditions are the same as those in Fig. 4. The blowing/suction rate varies from $\eta = 0$ to $0.0548/-0.0548$.

Fig. 5 illustrates the blowing effect on the axial-vel-

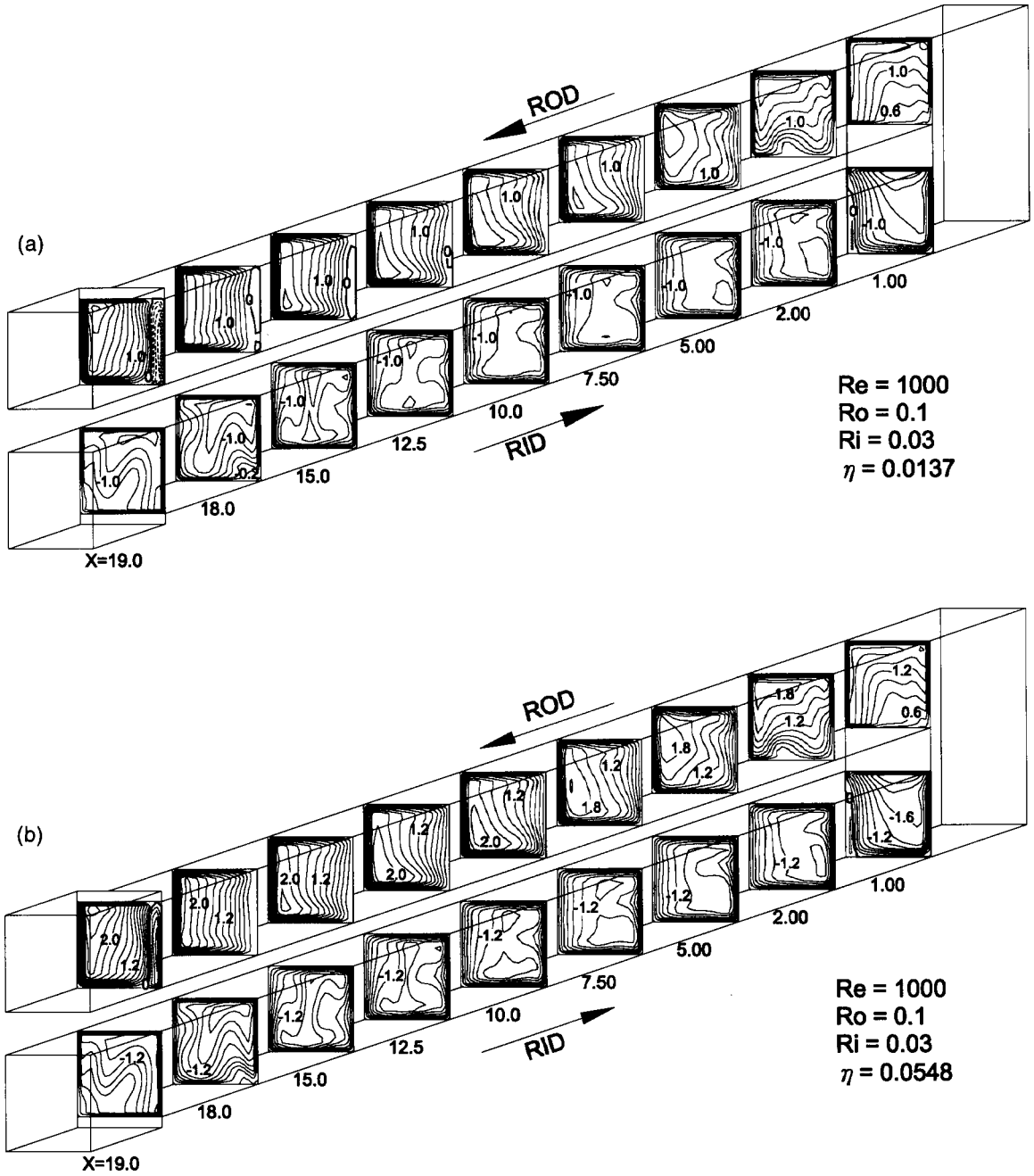

Fig. 5. Wall-blowing effect on the development of axial flow along the distance of the radial straight ducts for (a) $\eta = 0.0137$, $Ri = 0.03$, $Ro = 0.1$ and $Re = 1000$, (b) $\eta = 0.0548$, $Ri = 0.03$, $Ro = 0.1$ and $Re = 1000$.

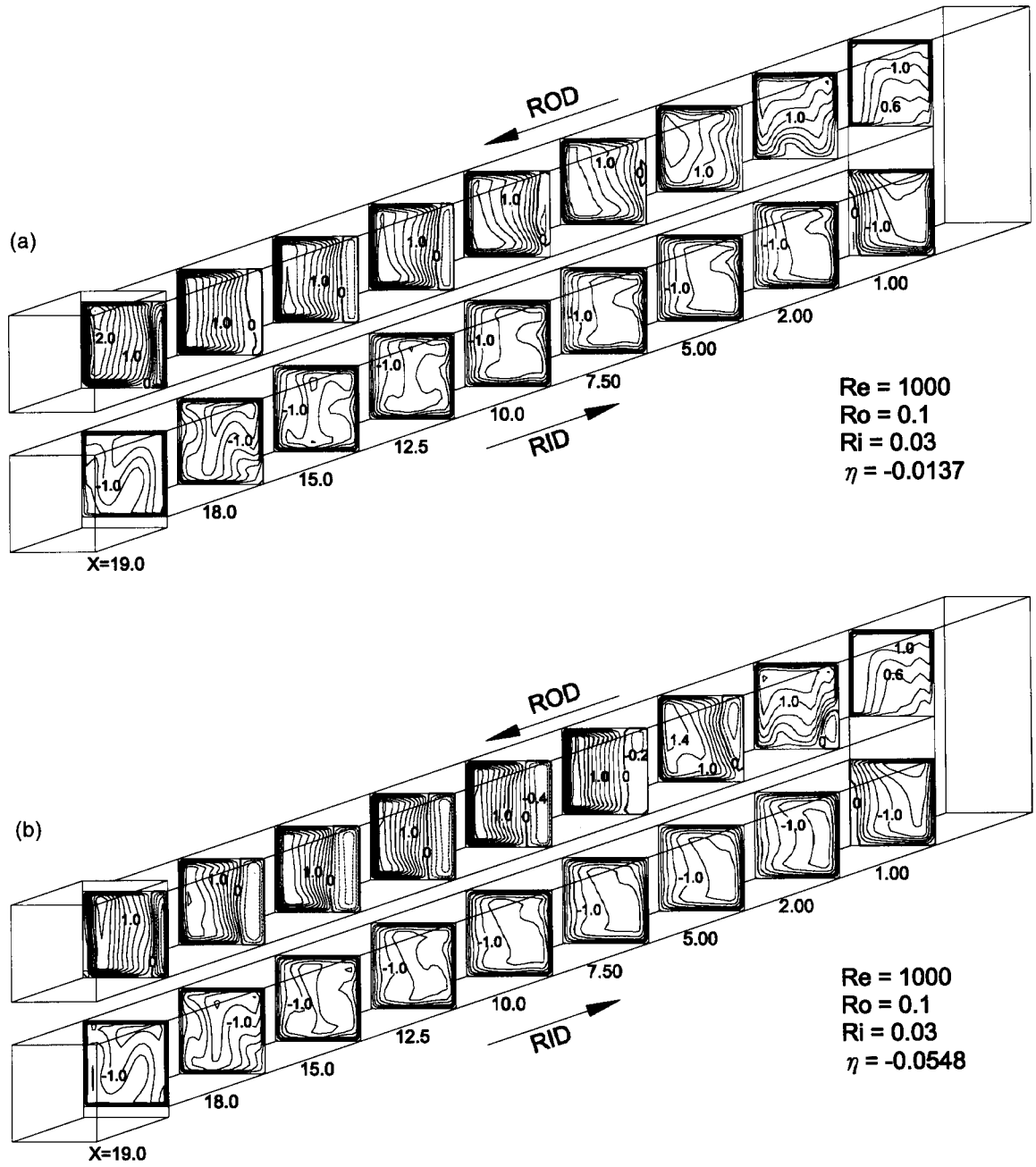

Fig. 6. Wall-suction effect on the development of axial flow along the distance of the radial straight ducts for (a) $\eta = -0.0137$, $Ri = 0.03$, $Ro = 0.1$ and $Re = 1000$, (b) $\eta = -0.0548$, $Ri = 0.03$, $Ro = 0.1$ and $Re = 1000$.

ocity development in the two-pass duct. Focus is first put on the flow-reversal phenomena in the ROD. At $\eta = 0.0137$ (Fig. 5(a)), the flow reversal at $X = 12.5$ of the ROD is smaller than that in Fig. 4, indicating that the flow separation from the leading wall has been delayed by the wall blowing. It can be observed more clearly by increasing the blowing rate to $\eta = 0.0548$, as shown in Fig. 5(b). The flow-reversal phenomena are not observed in the entire ROD except for the location adjacent to the sharp return. Contrarily, when the fluid is sucked away from the radial duct (Figs. 6(a) and (b)), the flow-reversal phenomena in the ROD become severe. At $\eta = -0.0137$, the radial flow separates from the leading wall of the ROD at the location between

$X = 5.0$ and 7.5. When the suction rate increases to $\eta = -0.0548$, the flow reversal occurs everywhere in the ROD. As for the results in the RID, both the wall-blowing and wall-suction effects on the axial-velocity development in the RID seem to be less significant than that in the ROD. At the most, the maximum radial velocity is increased/decreased slightly by increasing the blowing/suction rates.

A comparison of the cross-flow structure at mid-duct station ($X = 10$) for three different leading-wall conditions is shown in Fig. 7. Figs. 7(a)–(c) are the results of $\eta = 0$, 0.0545, and -0.0545, respectively. At $\eta = 0$, the secondary-flow structures shown in the RID and ROD (Fig. 7(a)) are quite different due to the buoyancy effect on the flow of different radial directions [20]. Nevertheless, the Coriolis force induced vortex pair is still observed in these two graphs. They circulate from the leading/trailing wall to the trailing/leading wall via the duct center and then return back along two sidewalls of the ROD/RID. Notably small intensity and random direction of the cross flow near the leading wall of the ROD is because of the existence of reversed flow (Fig. 4). When the fluid is injected into the radial duct through the leading wall (Fig. 7(b)), the direction of wall velocity in the ROD is coincident with the Coriolis force, which pushes the fluid from the leading wall toward the trailing wall. The Coriolis force induced vortex pair is thus enhanced, and the small cross-flow intensity near the leading wall is improved. Most importantly, the flow reversal at the corresponding location has been eliminated (Fig. 5(b)). As for the effect of wall suction on the secondary flow structure in the ROD (Fig. 7(c)), accordingly, the wall velocity is against the Coriolis force and thus dismisses the cross flow intensity. Interestingly, the original vortex pair caused by the forward flow has been placed to the trailing wall and an additional counter-rotating vortex pair at the two corners besides the leading wall has occupied about one-third duct cross section, which results from the reversed-flow induced Coriolis force. In contrast to the ROD's results, blowing/suction on the leading wall of the RID opposes/assists the Coriolis force. Although it is relatively small compared to the local cross-flow intensity and does not change the primary flow (Fig. 6) too much, the heat transfer characteristics are to a certain extent affected by the wall suction effect. This will be shown in the temperature-profile results later.

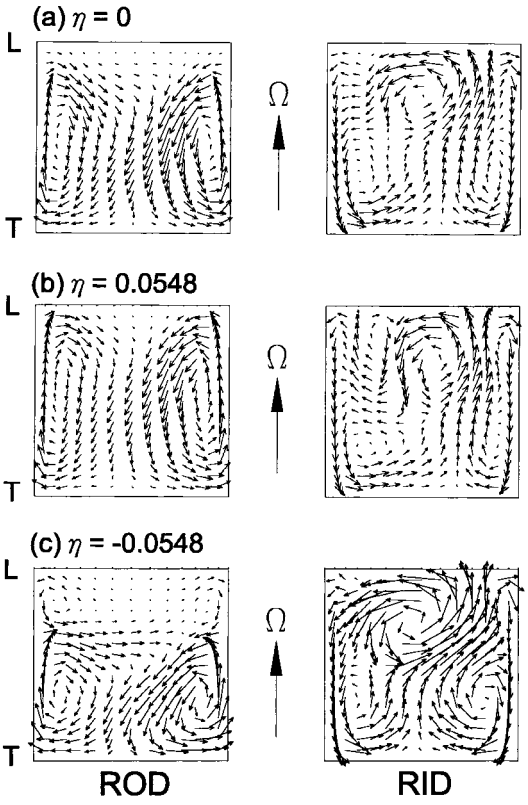

Fig. 7. Secondary-flow vectors for $Re = 1000$, $Ri = 0.03$ and $Ro = 0.1$ at axial station $X = 10$: (a) $\eta = 0$; (b) $\eta = -0.0548$; (c) $\eta = 0.0548$.

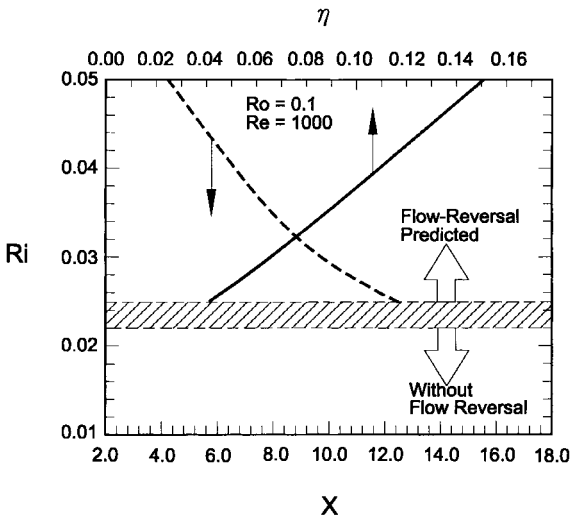

Fig. 8. Blowing rate for eliminating the flow reversal under various buoyancy forces.

Fig. 8 shows the requirement of the blowing rate on the leading wall to eliminate the flow reversal as a function of the Richardson number. The Reynolds number and the rotation number are fixed at $Re = 1000$ and $Ro = 0.1$, respectively. It can be seen that, at a fixed rotation speed of $Ro = 0.1$, the against buoyancy required to drive the radial flow inward in the ROD is about $Ri > 0.025$. When $Ri < 0.022$, the flow reversal is not predicted in the ROD. The dashed

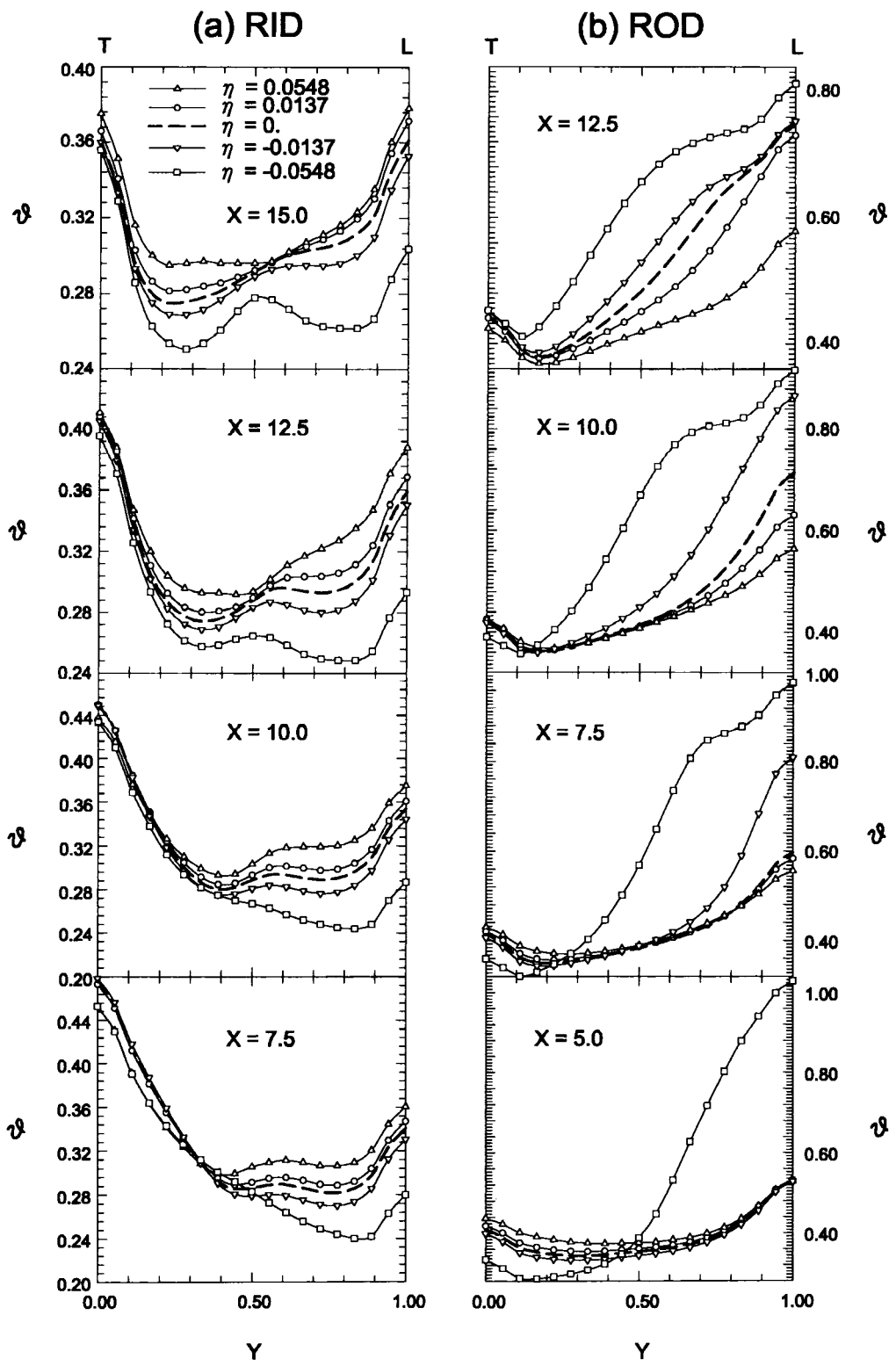

Fig. 9. Effect of blowing/suction rate on the temperature profiles across the centerline between the trailing and leading walls.

curve represents the radial distance from $X = 0$ to the initiation of flow reversal on the leading wall of the ROD at $\eta = 0$. It can be seen that the radial distance for initiation of flow separation decreases by increasing the Richardson number. This is because a duct with a lower wall heat flux at a fixed rotating speed requires a longer radius of radial rotation for reaching enough against buoyancy to drive the fluid upstream. It is further seen from this figure that the blowing rate required preventing the flow reversal increases by increasing the Richardson number.

3.3. Temperature profiles

Figs. 9(a) and (b), respectively, show the temperature profiles cutting across the centerlines of the RID ($Z = 0.5$) and the ROD ($Z = 2.0$) between the high- and low-pressure surfaces at several axial stations under various blowing/suction rates. The solid-walled results ($\eta = 0$, dashed line) are also displayed as a dashed curve for comparison. The Richardson number, Reynolds number and rotation number are fixed at $Ri = 0.03$, $Re = 1000$, and $Ro = 0.1$, respectively. The letters L and T in this figure denote the leading wall and the trailing wall, respectively. In the RID of $\eta = 0$ (Fig. 9(a)), the trailing-wall temperature and its increase rate along the radial distance are higher than those on the leading wall. The ROD has a reverse trend (Fig. 9(b)). Notably, a sharp increase in the leading-wall temperature from $X = 7.5$ to 10.0 indicates that the radial flow has a transition from outward to inward at about $X = 10$. Again, the thermal-fluid phenomena above results from the rotation-induced Coriolis force, buoyancy force, and their interaction [20].

As for the η effect, the leading-wall temperature in the RID (Fig. 9(a)) is reduced/increased by increasing the suction/blowing rates. When fluid is sucked away from the RID through the leading wall, the core flow of relatively low temperature is somewhat pulled toward the leading wall, and thus reduces the boundary layer on the leading wall. In addition, the direction of leading-wall velocity (v_w) is in parallel with and subsequently adds the rotational induced Coriolis force that enhances the cross flow (Fig. 7). Both these two effects reduce the leading-wall temperature. On the contrary, blowing acts against the Coriolis force, enlarges the boundary layer, and hence increases the leading-wall temperature of the RID. On the trailing wall of the RID, however, neither blowing nor suction significantly affects the wall temperature.

In contrast to the results in the RID, blowing and section respectively reduces and raises the leading-wall temperature in the ROD (Fig. 9(b)). The blowing flow on the leading wall assists the Coriolis force to drive the primary vortex pair (Fig. 7). In addition, it pushes the relatively warm fluid far away from the leading wall that reduces the local buoyancy; hence, more uniform temperature profiles. Both the above two effects reduce the leading-wall temperature. Contrarily, suction counteracts the Coriolis force, increases local buoyancy near the leading wall, and subsequently increases the leading-wall temperature. It should be noted that sharp increases in leading-wall temperature, e.g., from $X = 5.0$ to 7.5 for $\eta = -0.0137$ and from $X = 10.0$ to 12.5 for $\eta = 0.0137$, indicate the occurrence of flow separation from the leading wall of the ROD.

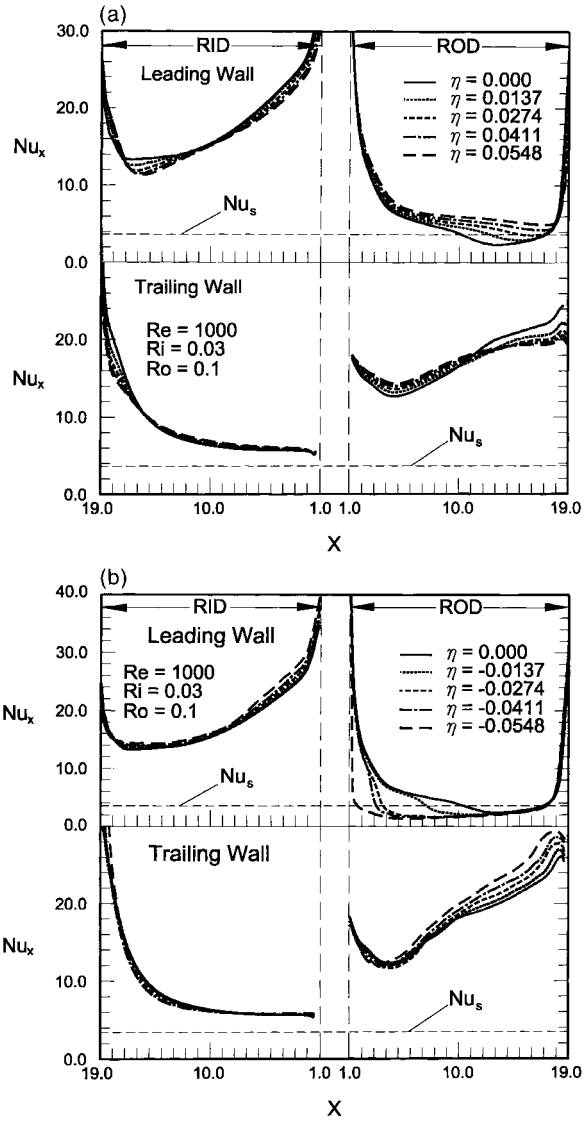

Fig. 10. (a) Effect of blowing rate on the local Nusselt number distribution on the leading and trailing walls. (b) Effect of suction rate on the local Nusselt number distribution on the leading and trailing walls.

Whenever the blowing rate is high enough to hinder the local buoyancy from driving the fluid upstream, say $\eta = 0.0548$, the flow reversal phenomena and subsequently local hot spots will be prevented in the entire ROD.

3.4. Nusselt number distributions

To evaluate the heat transfer performance, the computations of Nusselt numbers are of practical importance. Following the conventional definitions, the local spanwise-averaged (Z) Nusselt number of the leading and trailing walls is defined as follows:

$$Nu_x = q_w\, De/[k_f\,(T_w - T_b)] = 1/(\vartheta_w - \vartheta_b) \qquad (13)$$

Figs. 10(a) and (b), respectively, show the effects of blowing and suction on the local Nusselt number distributions along axial distance of the leading and trailing walls. The Reynolds number, rotation number and Richardson number are fixed at $Re = 1000$, $Ro = 0.1$ and $Ri = 0.03$, respectively. The dashed line and the solid curve in each graph represent the value of fully developed stationary flows (i.e., $Nu_s = 3.61$) and the solid-walled results, respectively. General trends show that, due to the Coriolis-force effect, the high-pressure surfaces have higher heat transfer coefficients than the low-pressure surfaces. In addition, owing to nearly stagnant main and cross flows (Figs. 6 and 7), the heat transfer coefficients on the leading wall of the ROD are very small, and even lower than Nu_s [20].

In the RID, the leading-wall Nusselt numbers

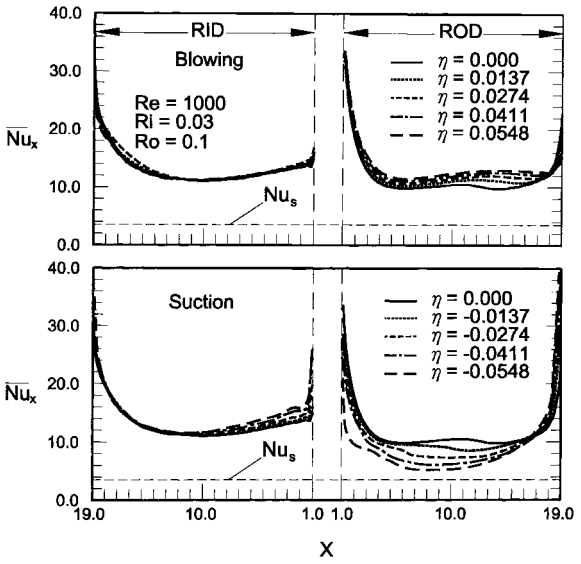

Fig. 11. Effect of blowing/suction rate on the distribution of peripherally averaged Nusselt number in the RID and ROD.

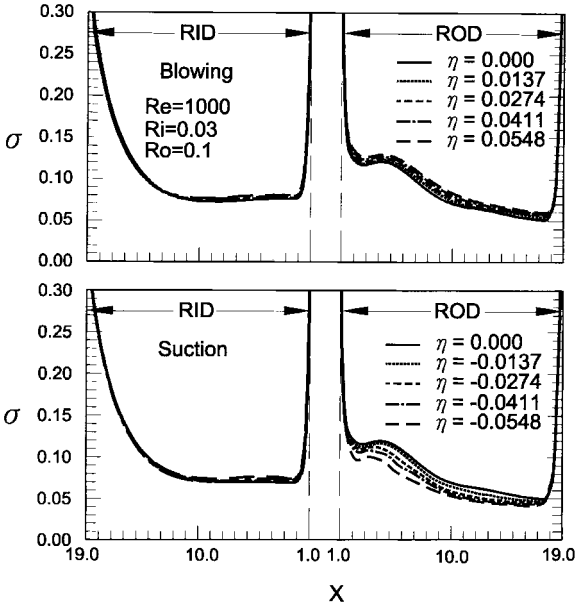

Fig. 12. Effect of blowing/suction rate on the cross-flow intensity distribution in the RID and ROD.

decrease/increase with increasing blowing/suction rates. The reasons have been explained in the temperature profiles above. In fact, the tendency is similar to that of the boundary layer on the flat plate with wall suction and blowing [30]. In general, suction thins the boundary layer and greatly increases the heat transfer, while blowing thickens the boundary layer and decreases the heat transfer. In the ROD, poor heat transfer on the leading wall has been improved gradually by the wall blowing but has been degraded further by the wall suction. Significantly low heat transfer do not occur in the entire ROD for $\eta \geqq 0.0411$.

Fig. 11 shows the distributions of peripherally (four-wall) averaged heat transfer coefficient ($\overline{Nu}_x$) along the RID and ROD. It is seen that the blowing and suction respectively augments and degrades the peripherally averaged heat transfer in the ROD, but they negligibly affect the $\overline{Nu}_x$ distribution in the RID. Since the $\overline{Nu}_x$ development in the buoyancy-affected ROD and RID parallels with the cross-flow-intensity development [20], it is important to know whether this tendency is true by considering the transpiration effect. Fig. 12 shows the distributions of the cross-sectional averaged cross-flow intensity along the RID and ROD under various η. The cross-flow intensity at any axial location is defined as

$$\sigma = \int_0^1 \int_0^1 \sqrt{V^2 + W^2}\, \mathrm{d}Y\, \mathrm{d}Z \quad \text{for the RID} \qquad (14.1)$$

$$= \int_{1.5}^{2.5}\int_{0}^{1} \sqrt{V^2 + W^2}\, dY\, dZ \quad \text{for the ROD} \qquad (14.2)$$

From Fig. 12, it can be seen that leading-wall blowing and suction respectively promotes and depresses the cross-flow intensity in the ROD, but neither of them affect significantly the σ development in the RID. The simulation of the η dependence of $\overline{Nu}_x$ and that of σ has given a verification of the above explanation of the mechanisms of heat transfer augmentation or degradation due to the leading-wall blowing/suction in the multiple-pass rotating duct.

4. Summary and conclusions

The effect of wall blowing/suction on mixed convective heat transfer in a radially rotating multiple-pass duct has been investigated numerically. Uniform fluid is injected into or sucked away from the radial duct through the leading wall. The mechanisms of heat transfer augmented or degraded by the effects of wall blowing and suction in the RID and ROD are examined, discussed and compared thereafter. Main findings based on the present study are as follows:

1. Under the solid wall conditions, the radial distance for initiation of flow separation in the ROD decreases by increasing the Richardson number. This is because in a duct with a higher wall heat flux at a fixed rotating speed, only a shorter radius of radial rotation is required for reaching an enough against buoyancy to drive the fluid upstream.
2. Leading-wall blowing can retard the flow separation in the ROD, but leading-wall suction has an inverse effect. The blowing rate required for preventing the flow reversal in the ROD increases by increasing the Richardson number.
3. In the ROD, the leading-wall blowing assists the Coriolis force that enhances the cross-flow intensity, pushes the relatively warm fluid far away from the leading wall that reduces the local against buoyancy, and thus reduces the leading-wall temperature. Contrarily, suction counteracts the Coriolis force, increases the local against buoyancy, and subsequently increases the leading-wall temperature. In the RID, blowing and suction on the leading wall have the adverse effects on the leading-wall temperature. On the trailing wall of the ROD and RID, however, neither blowing, nor suction affects the wall temperature significantly.
4. In the ROD, the significantly poor heat transfer on the leading wall has been improved gradually by the leading-wall blowing but has been degraded further by the leading wall suction.
5. Leading-wall blowing and suction respectively augments and degrades the peripherally averaged heat transfer $\overline{Nu}_x$ in the ROD, but neither significantly affects the $\overline{Nu}_x$ distribution in the RID. Similar effects of wall blowing and suction on the cross-flow intensity development is observed in the ROD and RID. This is just an explanation of the mechanisms in heat transfer enhancement by wall blowing or suction in the RID and ROD.

Acknowledgement

Support for this work was provided by the National Science Council of the Republic of China under Contract No. NSC 85-2212-E-216-003.

References

[1] J.E. Hart, Instability and secondary motion in rotating channel flow, J. Fluid Mech. 45 (1971) 337–395.
[2] H. Ito, K. Nanbu, Flow in rotating straight pipes of circular cross-section, Trans. ASME, Journal of Basic Eng. Power 94 (1972) 261–270.
[3] J. Moore, A wake and eddy in a rotating, radial-flow passage, Part 1: experimental observation, J. Engng Power 95 (1973) 205–212.
[4] J. Moore, A wake and eddy in a rotating, radial-flow passage, Part 2: flow model, J. Engng Power 95 (1973) 213–219.
[5] C.G. Spezial, S. Thangam, Numerical study of secondary flow and roll-cell instabilities in rotating channel flow, J. Fluid Chem. 130 (1983) 337–395.
[6] H.S. Kheshgi, L.E. Scriven, Viscous flow through a rotating square channel, Phys. Fluids 28 (1985) 2968–2979.
[7] W.D. Morris, Heat Transfer and Fluid Flow in Rotating Coolant Channels, John Wiley and Sons, New York, 1970.
[8] W.D. Morris, T. Ayhan, Observation in the influence of rotation on heat transfer in the coolant channel of gas turbine rotor blade, Proc. Inst. Mech. Engrs 193 (1979) 303–311.
[9] R. Siegle, Analysis of buoyancy effect on fully developed laminar heat transfer in a rotating core tube, Trans. ASME, J. Heat Transfer 107 (1985) 338–344.
[10] G.J. Hwang, T.C. Jen, Convective heat transfer in rotating isothermal ducts, Int. J. Heat Mass Transfer 33 (1990) 1817–1828.
[11] J.H. Wagner, B.V. Johnson, T.J. Hajek, Heat transfer in rotating passages with square smooth walls and radial outward flow, Trans. ASME, J. Turbomachinery 113 (1991) 42–51.
[12] C.Y. Soong, S.T. Lin, G.J. Hwang, An experimental study of convective heat transfer in radial rotating rectangular ducts, Trans. ASME, Journal of Heat Transfer 113 (1991) 604–611.
[13] T.C. Jen, A.S. Lavine, G.J. Hwang, Simultaneously developing laminar convection in rotating isothermal

square channels, Int. J. Heat Mass Transfer 35 (1992) 239–254.
[14] S. Fann, W.J. Yang, Hydrodynamically and thermally developing laminar flow through rotating channels having isothermal walls, Numerical Heat Transfer, Part A 22 (1992) 257–288.
[15] J.C. Han, Y.M. Zhang, Effect of uneven wall temperature on local heat transfer in a rotating square channel with smooth walls of radial outward flow, Trans. ASME, J. Heat Transfer 114 (1992) 850–858.
[16] J.H. Wagner, B.V. Johnson, F.C. Kopper, Heat transfer in rotating serpentine passages with smooth walls, Trans. ASME, J. Turbomachinery 113 (1991) 321–330.
[17] J.H. Wagner, B.V. Johnson, R.A. Grazinani, F.C. Yeh, Heat transfer in rotating serpentine passages with trips normal to the flow, Trans. ASME, J. Turbomachinery 114 (1992) 847–857.
[18] W.J. Yang, N. Zhang, J. Chiou, Local heat transfer in a rotating serpentine flow passage, Trans. ASME, J. Heat Transfer 114 (1992) 354–361.
[19] G.J. Hwang, C.R. Kuo, Experimental studies and correlations of convective heat transfer in a radially rotating serpentine passage, Trans. ASME, J. Heat Transfer 119 (1997) 460–466.
[20] J.J. Hwang, D.Y. Lai, Three dimensional mixed convection in a rotating multiple-pass square channel, Int. J. Heat Mass Transfer 41 (1998) 979–991.
[21] J.J. Hwang, D.Y. Lai, Three dimensional laminar flow in a rotating multiple-pass square channel with sharp 180-deg. turns, Trans. ASME, J. Fluids Engineering 120 (1998) 488–495.
[22] C.Y. Soong, G.J. Hwang, Laminar mixed convection in a radially rotating semiporous channel, Int. J. Heat Mass Transfer 33 (1990) 1805–1816.
[23] W.M. Yan, Developing flow and heat transfer in radially rotating rectangular ducts with wall-transpiration effects, Int. J. Heat Mass Transfer 37 (1994) 1465–1473.
[24] W.M. Yan, Effects of wall transpiration on mixed convection in a radial outward flow inside rotating duct, Int. J. Heat Mass Transfer 37 (1994) 1465–1473.
[25] C.V. Prakash, R. Zerkle, Prediction of turbulent flow and heat transfer in a radially rotating square duct, Trans. ASME, J. Turbomachinery 114 (1992) 835–846.
[26] S.V. Patankar, L.H. Liu, E.M. Sparrow, Fully developed flow and heat transfer ducts having periodic variations of the cross-sectional area, Trans. ASME, J. Heat Transfer 99 (1977) 180–186.
[27] S.V. Patankar, Numerical Heat Transfer and Fluid Flow, Hemisphere, Washington, DC, 1980.
[28] J.P. Van Doormaal, G.D. Raithby, Enhancements of the SIMPLE method for predicting incompressible fluid flows, Numerical Heat Transfer, Part A 7 (1992) 147–163.
[29] J.J. Hwang, T.Y. Lia, S.H. Chen, Predictions of turbulent fluid flow and heat transfer in a rotating periodical two-pass square duct, International Journal of Numerical Methods for Heat and Fluid Flow 8 (1998) 519–538.
[30] H. Schlichting, Boundary Layer Theory, McGraw-Hill, New York, 1979.